Templating of Self-Alignment Patterns of Anisotropic Gold Nanoparticles on Ordered SWNT Macrostructures

Budhadipta Dan,[†,§] Tyler B. Wingfield,[§] Julian S. Evans,[§] Francesca Mirri,[‡] Cary L. Pint,[†] Matteo Pasquali,[‡,*] and Ivan I. Smalyukh[§,⊥,*]

[†]Department of Physics and Astronomy, [‡]Department of Chemical and Biomolecular Engineering, and Department of Chemistry, R.E. Smalley Institute for Nanoscale Science & Technology, Rice University, 6100 Main Street, Houston, Texas 77005, United States

[§]Department of Physics and Liquid Crystal Materials Research Center, University of Colorado, 2000 Colorado Ave, Boulder, Colorado 80309, United States

[⊥]Renewable and Sustainable Energy Institute, University of Colorado and National Renewable Energy Laboratory, Boulder, Colorado 80309, United States

S *Supporting Information*

ABSTRACT: We report a simple and versatile technique for oriented assembly of gold nanorods on aligned single-walled carbon nanotube (SWNT) macrostructures, such as thin nanotube films and nanotube fibers. The deposition and assembly is accomplished via drop drying of dilute gold nanorod suspensions on SWNT macrostructures under ambient conditions. Guided by anisotropic interactions, gold nanorods, and polygonal platelets spontaneously align with SWNTs, resulting in macroscopic arrays of locally ordered nanorods supported on aligned SWNT sub-

strates. SEM reveals that the scalar order parameter of rods relative to the local average SWNT alignment is 0.7 for rods on SWNT films and 0.9 for rods on SWNT fibers. This self-alignment is enabled by anisotropic gold nanoparticle—SWNT interactions and is observed for a wide range of nanoparticles, including nanorods with aspect ratios ranging from 2—35, thin gold triangular and other polygonal platelets. The plasmonic properties of aligned gold nanorods together with superior electronic, chemical and mechanical properties of SWNTs make these hybrid nanocomposites valuable for the design of self-assembled multifunctional optoelectronic materials and optical metamaterials.

KEYWORDS: gold nanorods, SWNT, films, fibers, template, aligned arrays
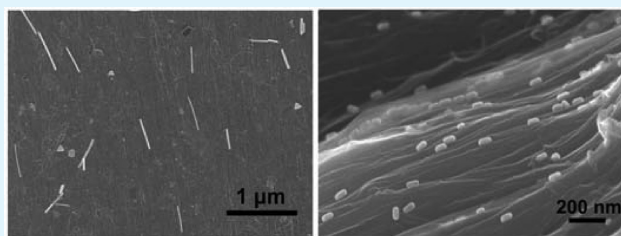
Metallic nanoparticles have been the subject of intense research because of their unusual electro-optical properties and a broad range of potential applications.[1,2] Current research toward nanoparticles for metamaterial applications is primarily focused in two directions: synthesis and ordered assembly. Synthesis involves designing new methods for fabrication of nanoparticles from a variety of materials, with varied anisotropic shapes, sizes, and aspect ratios. Particles are being tailored to possess highly tunable plasmonic and optoelectronic properties aimed for specific advanced applications. Ordered assembly entails deposition of nanoparticles on surfaces, incorporation into bulk liquid crystalline media, or chemically mediated crystallization in an organized manner so as to leverage the unique properties of individual nanoparticles collectively and attain functional behavior on macroscopic scales. Gold nanorods (GNRs) and polygonal nanoplatelets are a particularly interesting class of nanoparticles because their surface plasmon resonance (SPR) depends on polarization and can be tuned across the visible and near IR spectrum by changing the GNR aspect ratio.[3] Promising GNR applications include plasmonic enhancement of photoconversion in photovoltaics,[4−6] surface enhanced Raman scattering (SERS)-based detection and imaging,[7,8] biological

imaging and therapy,[9−11] and optical metamaterials;[12,13] large-scale ordered assembly of GNRs is a critical step for the development of many of these applications.

Recent advances in ordered assembly and nanoscale alignment of GNRs include incorporation into lyotropic liquid crystals,[12] stretched polymer films,[14,15] electric field driven alignment in a liquid medium,[16] colloidal self-assembly,[17,18] and deposition onto patterned surfaces.[19] In most cases, however, the substrates or surrounding material (for bulk incorporation) possess minimal or no functionality; the lack of essential properties like electrical conductivity, mechanical strength, or chemical durability often limits the range of possible applications for these hybrid materials.

Single-walled carbon nanotubes (SWNTs) offer a promising alternative in this context. SWNTs offer the functional and structural features of high performance polymers,[20] coupled with superior electro-optical properties and chemical inertness.[21] Their nanoscale diameter combined with high aspect ratio
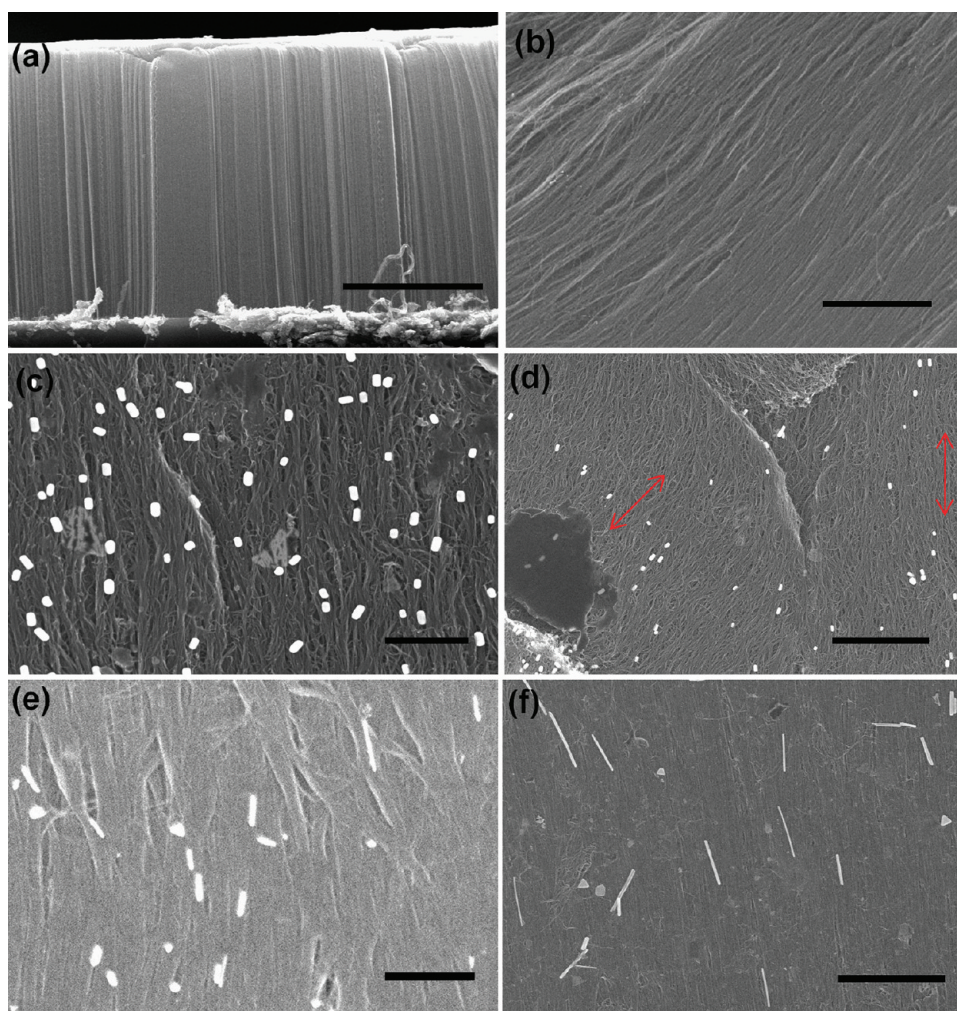
Figure 1. SEM of macroscopic ordered assemblies of gold nanorods (GNRs) of varying aspect ratios, produced by drop drying on aligned SWNT films. (a) Vertically aligned SWNT carpet. (b) Aligned SWNT film fabricated from SWNT carpet. (c) Spontaneous alignment of short GNRs (aspect ratio 2−4) on SWNT film. (d) GNRs replicating the alignment defect in underlying film (shown with red arrows). (e, f) Alignment of medium (5−12) and long (12−35) aspect ratio GNRs with SWNTs. Scale bars: (a) 15 μm, (b) 1 μm, (c) 400 nm, (d) 1 μm, (e) 500 nm, (f) 1 μm.

(>1000) makes them ideal candidates for forming high performance thin films[22,23] and fibers,[24−27] which in turn serve as basic functional materials for a host of engineering applications, devices and materials. For example, SWNT thin films are being developed as transparent conductive coatings for touch screens, flat electronic displays, OLEDs, electrodes for solar cells, etc.[28,29] High specific surface area, ~1300 m^2/g,[30] makes SWNT macrostructures highly desirable substrates for hosting other functional nanoparticles, for example, SWNT-based supports for catalyst nanoparticles, SWNT electrodes for fuel cells,[31,32] and oriented attachment of GNRs on sidewalls of individual polymer coated multi-walled nanotubes (MWNTs).[33]

In this article, we report the spontaneous ordered deposition of plasmonic GNRs and polygonal platelets on various highly aligned SWNT macrostructures. We employ a simple "drop drying" method, which utilizes anisotropic physical interactions between GNRs and SWNT structures including capillary, entropic, van der Waals forces, and the co-operative interplay among them. The method successfully achieves "templated" deposition of GNR arrays over large length scales (~millimeters) on planar as well as curved SWNT substrates. The
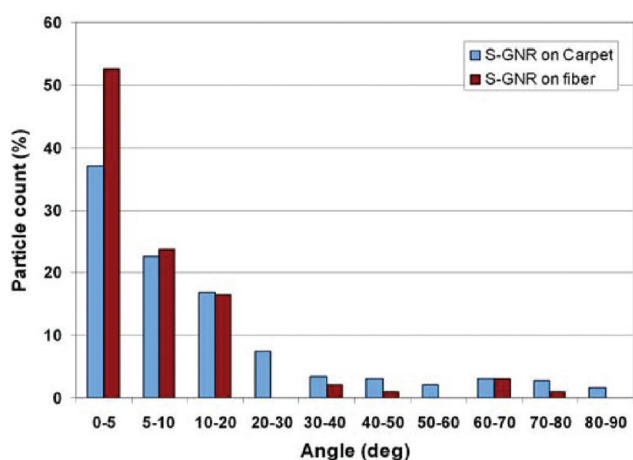
superior electro-optical properties of SWNTs coupled with optical properties of plasmonic nanoparticles make SWNT−GNR composites potential candidates for a number of optoelectronic applications like electrodes for light harvesting devices, electrochemical cells, conductive platforms for plasmon-enhanced imaging.

■ RESULTS AND DISCUSSION

The GNR deposition process consisted of drop drying GNR colloidal suspensions (few microliters) on top of the aligned SWNT macrostructures; the process was demonstrated on films and fibers made of highly aligned SWNTs. Upon completion of drying under ambient conditions, the samples were further heated to ~90 °C for 5 min to ensure complete removal of the solvent. The desired density of GNRs on SWNT films and fibers was achieved by repeating the drop drying procedure multiple times. GNRs with a wide range of aspect ratios (~2−35) were deposited on SWNT films using this procedure. The deposition on SWNT fibers was performed with short GNRs suspended in two different types of media, aqueous and an organic solvent (ethanol). Both types of suspensions yielded similar results.
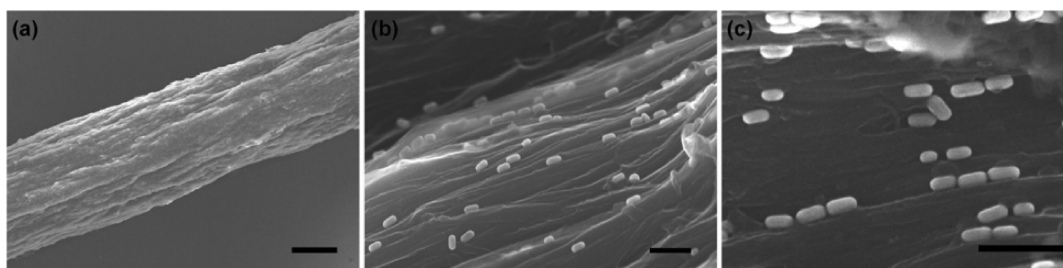
Figure 2. SEM image of (a) SWNT fiber and (b, c) spontaneous alignment of short GNRs with SWNTs in the fiber. GNRs were deposited onto the fiber by drop drying as well as dip coating, both methods producing similar results. Scale bars: (a) 40 μm and (b, c) 200 nm.

Figure 3. Orientational distribution function for spontaneously aligned short GNRs (S-GNRs) on aligned SWNT macrostructures. Orientation "angle" for each GNR was calculated with respect to the underlying SWNT/SWNT bundle. Total of 322 particles were analyzed for S-GNRs on SWNT carpets, and 97 particles for S-GNRs on SWNT fibers.

Table 1. 2D scalar order parameter values for ordered arrays of GNRs with varying aspect ratios, deposited on highly aligned SWNT films, and short GNRs on fibers

films		fibers	
GNR aspect ratio	order parameter	GNR aspect ratio	order parameter
2—4	0.73	2—4	0.87
5—12	0.70		
12—35	0.73		

larger), but show considerable waviness and undulations at shorter length scales (tens of nanometers), that can be described by a local direction of SWNT alignment, $N_{SWNT}(r)$. Better unidirectional global alignment could be obtained by improving the alignment of the SWNTs and SWNT bundles in the substrates. An example of large area aligned GNR deposition on a well-aligned macroscopic SWNT fiber is shown in the Supporting Information (Figure S2).

GNR alignment on SWNT macrostructures was quantified by measuring the angular orientation of individual GNRs with respect to the aligned SWNTs in the SEM images. Multiple SEM images were analyzed for each GNR type (short, medium, and long) to collect data for statistically significant number of GNRs. For example, a total of 322 short GNR particles were analyzed for SWNT films and 97 particles for short GNRs on SWNT fibers. In order to estimate the degree of relative alignment of GNRs and SWNTs, the angular orientation of individual GNRs (defined as "α") was measured with respect to the direction of alignment N_{SWNT} of the locally underlying SWNTs ($\alpha = 0$). This analysis of substrate-induced alignment of GNRs is similar to the analysis of ordering of dye molecules and anisotropic particles imposed by the elasticity of liquid crystal host media, (for example, see refs 34—36) where the order parameters of aligned dye molecules or rods were also probed with respect to the local director of the surrounding liquid crystal. Figure 3 shows the normalized orientation distribution function obtained for short GNRs deposited on aligned SWNT carpet films and SWNT fibers. Higher aspect ratio GNRs deposited on SWNT films showed a similar angular distribution. The standard deviation and standard error in measurements of α are provided in the Supporting Information.

The angular orientation measurements for individual GNR particles were used to calculate the 2D scalar order parameter (S_{2D}) for GNR arrays deposited on SWNT macrostructures. S_{2D} was obtained by evaluating $2\langle \cos^2 \alpha \rangle - 1$ for each GNR and taking an average over all GNRs belonging to each aspect ratio

The GNR—SWNT composites were analyzed using SEM imaging. Remarkably, we found that a large fraction of GNRs spontaneously align along the SWNTs in the films and fibers during the deposition process, as shown in Figure 1c—f and Figure 2b—c. In addition, the strong spontaneous alignment to the SWNT substrate was observed for all GNR aspect ratios. Most of the nonaligned GNRs were within rare aggregates. Nonuniformities (cracks, sharp protrusions, misaligned domains and domain boundaries, etc.) in the underlying SWNT macrostructure promoted aggregation and accumulation of GNRs, often leading to their nonuniform distribution. Employing dilute GNR suspensions limited the extent of GNR aggregation during drop drying and yielded an ordered and oriented GNR deposition.

Closer inspection of certain regions in GNR-SWNT thin films with imperfect alignment, like in Figure 1d, reveals that the GNRs closely follow the local SWNT alignment and therefore reproduce the defects and distortion patterns in their underlying SWNTs. This shows the effectiveness of this technique as a templating mechanism, which can be employed to replicate varied and intricate patterns from underlying SWNT substrates to the deposited GNR layer. Because of the same effect, the GNR arrays deposited on the films and fibers shown in Figure 1 are less ordered on large length scales. In the films and fibers used here, SWNTs are aligned over large length scales (micrometers and
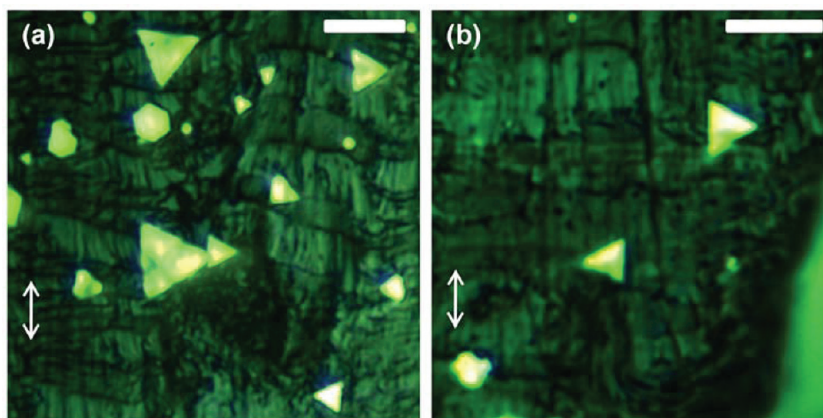
3720

dx.doi.org/10.1021/am2009019 |ACS Appl. Mater. Interfaces 2011, 3, 3718–3724

Figure 4. (a, b) Optical images (reflection mode, $50\times$ lens) showing the spontaneous alignment of 2D gold triangles and platelets, with one side of each polygon aligned parallel to underlying SWNTs in aligned SWNT films. The direction of SWNT alignment is shown by double sided arrows. Scale bar is 10 μm in both images.

group. S_{2D} values obtained using this method of analysis "filter out" the effect of undulations imparted onto the GNR assembly becaue of alignment imperfections in the SWNT substrate, and indicate the degree of ordering achievable in a GNR array deposited on a perfectly aligned SWNT substrate with $N_{SWNT}(r) =$ constant. The values of S_{2D} listed in Table 1 further illustrate the high degree of spontaneous alignment among GNRs, imposed by the underlying ordered structures of SWNTs.

Interestingly, SWNT fibers produced better alignment and a higher order parameter among GNRs than the films. This is likely due to the "grooved" surface morphology of the fibers (groove width $\sim$ tens of nanometers), which are composed of substructures of smaller diameter SWNT ropes and fibrils. The unidirectional grooves which are comparable to the diameter of the GNRs but smaller than their length can exert entropic alignment forces, leading to better alignment and higher order parameter. The alignment of GNRs on SWNT fibers demonstrates the portability of this technique to other SWNT macrostructures, including curved surfaces. Since the alignment behavior of GNRs on SWNT films was independent of GNR aspect ratio, the deposition on fibers was tested with only short GNRs.

The self-alignment behavior during drop drying on SWNT substrates, was investigated also using suspensions of gold nanoparticles possessing other interesting shapes, like high-aspect-ratio triangles and polygonal platelets[37] (prepared using the procedures described in ref 38). Interestingly, a significant number of gold triangles and polygons spontaneously aligned during deposition, with one side of polygon parallel to the SWNT alignment direction (Figure 4). This demonstrates that alignment is not restricted to only rod shaped particles. The aligned triangles did not show any predominant polarity and the fraction of aligned nanoparticles was lower than that in the case of GNRs.

The spontaneous alignment of GNRs on aligned SWNT substrates is driven by anisotropic interactions between GNRs and SWNT structures; these interactions are a combination of capillary, entropic and van der Waals forces. During drop drying, GNRs become confined into a progressively thinning liquid film and are pushed closer to the liquid free surface as well as the anisotropic substrate. Under these circumstances, anisotropic capillary and combing forces may play an important role (Figure 5a). Assembly of colloidal particles mediated by capillarity and receding

contact lines has been reported before.[39] For drop drying on isotropic substrates, oriented assembly is typically restricted to drop edges.[36,40] In contrast, drop drying on anisotropic micro- and nanostructured surfaces can produce nanoscale orientation and uniform assembly on larger areas.[41−46] For example, minimization of surface free energy[41] and evaporation on surfaces with patterned hydrophobicity[42] has been used for alignment and ordered deposition of nanoparticles. Strano et al.[43] reported the role of hydrodynamic and capillary forces in the alignment, nanoscale positioning and deposition of individual SWNTs inside a cylindrical liquid droplet. Petit and Carbeck[44] reported the molecular combing in microchannels, where DNA molecules get oriented and stretched at the interface of liquid suspension and hydrophobic capillary substrate. Anisotropic capillary forces are used for the alignment and assembly of nanowires in device fabrication.[45,46]

In close proximity to the nanostructured SWNT substrate, overall translational and orientational entropy of GNRs is orientation dependent, which gives rise to entropic alignment forces. Spontaneous alignment on nanoscale grooved surfaces has been observed for liquid crystals (LCs) as well.[47] However, there are important differences between these two systems. For thermotropic small-molecule LCs with molecular dimensions of the order of 1 nm (typically several nanometers in length and subnanometer in width), the entropic effects can be neglected (the ensuing entropic interactions are much smaller than confinement-induced elastic forces and anisotropic van der Waals interactions of LC molecules with the surfaces). The entropic forces become important in lyotropic LCs composed of cylindrical micelles (surfactant-based LCs) or long molecular aggregates (chromonic LCs) that can have lengths comparable to that of our nanorods ($\sim$ 50 nm). However, the most important difference is that LCs, due to their bulk elasticity, exhibit coupling of the orientation of micelles and chromonic aggregates at the surface with the far-field director away from the surface, which is not the case for nanorods studied here. Our observations have closer resemblance to the entropy-mediated templating of patterns, from micro and nanostructured surfaces to colloidal particles in dilute suspension, observed in other systems.[48−50] Onsager theory[51] of nematic LCs describes the spontaneous ordering of colloidal rigid rods for minimization of excluded volume and maximization of entropy; in our case, similar interactions between each rigid rod and the features on
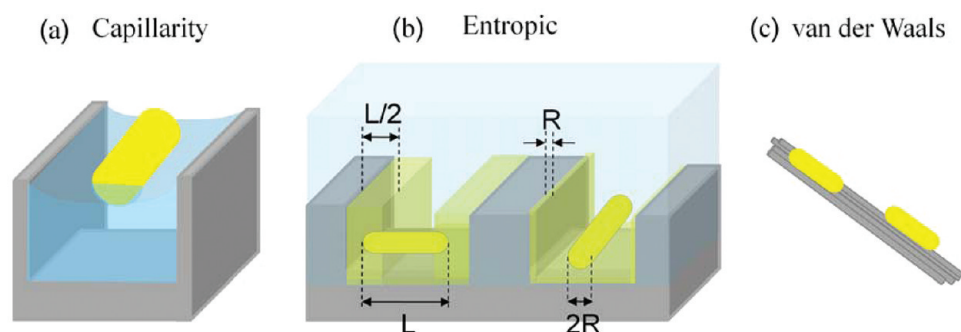
Figure 5. Various forces contributing to assembly and alignment of gold nanorods on SWNT substrates. (a) Capillarity: capillary forces promote alignment of nanorods to minimize distortions in the liquid free surface. (b) Entropic forces: aligning with SWNTs and nanochannels between SWNTs minimizes excluded volume (depicted by the shaded region, which are inaccessible by the rod center of mass) and maximizes entropy. (c) Anisotropic van der Waals interactions; by aligning with the SWNTs, nanorods maximize their area of contact and reduce free energy.

structured surfaces like walls of channels, protrusions and corners, help colloidal particles to attain well-defined positions and orientations. In the case of anisotropic colloids like GNRs, in unidirectional nanochannels created by SWNTs, alignment leads to reduction in their excluded volume by $\sim(L-2R)A$, where A is the surface area of channel-like substrate nanostructures, L is the length of a GNR, and R is its radius, as depicted in Figure 5b.

Finally, as GNRs deposit on the substrate, van der Waals interactions with individual SWNTs and SWNT bundles strongly affect their orientation, as depicted in Figure 5c. Aligning with SWNTs in the substrate allows GNRs to maximize their area of contact and achieve a lower energy state by means of increased van der Waals interaction. An important point to note here is that GNRs should have stronger van der Waals attraction toward each other than to SWNTs, because gold has a higher Hamaker constant than carbon. However, a stabilization layer of micellar Cetyl Trimethyl Ammonium Bromide (CTAB) on GNRs prevents their self-aggregation and flocculation in suspension, while allowing them to interact with bare uncoated SWNT surfaces during deposition. Using a high concentration GNR suspension during deposition, however, can lead to deposition of multiple layers of GNRs over the same spot. The secondary and more layers of GNRs may experience much weaker templating effect of the underlying SWNT.

Further insight into the relative influence of these three forces on the oriented assembly of GNRs was obtained from the deposition of short GNRs on SWNT fibers. Short GNRs suspended in two different media, aqueous and in an organic solvent, were deposited on SWNT fibers using the same procedure (shown in Figure 2 and Figure S3 in the Supporting Information, respectively). Because of the hydrophobic nature of SWNTs, GNRs in aqueous and organic suspensions will experience different wetting behavior, contact angle, and capillary forces. In addition, different stabilizing polymers/surfactants were employed to suspend the GNRs in the two different solvents. However, a similar degree of alignment was observed in both cases, which indicates the relative dominance of entropic forces in the GNR oriented assembly process; this is especially true for the case of SWNT fibers, which possess a grooved surface morphology as mentioned before.

Similar forces are possibly in play for the case of anisotropic gold platelets and polygons (Figure 4). In the simplest case, an anisotropic gold triangle or platelet (5 nm thick, 10 μm wide) approaching the SWNT film surface with its plane perpendicular to it locally resembles a GNR with 5 nm diameter. Thus, the interplay of various alignment forces leads to deposition of the triangle with one of the sides parallel to SWNT orientation. The interactions and reduction of free energy due to alignment become more complex for other possible plane orientations, which explains the lower fraction of aligned particles observed in the case of polygonal platelets, compared to GNRs.

■ CONCLUSIONS

We have demonstrated a drop-drying-based simple and versatile technique for the ordered assembly of gold nanoparticles on highly aligned SWNT films and fibers. The method was successfully demonstrated using GNRs with aspect ratios ranging from 2—35, gold triangles with side length up to 10 μm and 5 nm thickness, and other polygonal shapes. The nanoparticles show strong interaction with SWNTs, and spontaneously align on the anisotropic substrates during deposition. These ordered arrays of plasmonic GNRs supported on strong, durable, inert, and electrically conductive SWNT substrates can potentially better serve the currently existing GNR applications and act as a platform for development of advanced metamaterials.

■ MATERIALS AND METHODS

Anisotropic Gold Nanoparticle Fabrication. GNRs with medium ($\sim$5—12) and high aspect ratios ($\sim$12—35), were fabricated using standard seed mediated growth in the presence of CTAB (Cetyl trimethylammonium bromide).[2,17,18] Briefly, spherical gold seeds were produced by reducing chloroauric acid with sodium borohydride in the presence of CTAB. Next, three identical growth solutions were prepared with chloroauric acid, CTAB, and ascorbic acid. To produce medium length GNRs, we added the seed to the first solution and the reaction was allowed to take place progressively in each growth solution for a couple of hours, followed by pipet transfer to the next growth solution. To produce long rods, we allowed the reaction to proceed in the first two growth solutions for less than a minute and then left in the third solution overnight. In both cases, the final product was obtained in the form of a precipitate consisting of CTAB capped GNRs. The GNRs were recovered and redispersed to form dilute aqueous suspensions (1 mg/mL). Short GNRs (aspect ratio $\sim$2—4) were purchased from Nanopartz Inc. (Loveland, Colorado).

High aspect ratio, polydisperse gold triangular and other polygonal platelets with up to 10 μm side lengths and about 5 nm thickness were produced using an aloe vera extract technique: 30 g of aloe vera leaf were boiled in 100 mL of deionized water to produce the extract, 1 mL of the extract was then added to 1 mM chloroauric acid in 9 mL of methanol

and allowed to sit at room temperature for several days (for more details see refs 38 and 52).

Aligned SWNT Macrostructure Fabrication. Thin films of horizontally aligned SWNTs were prepared from vertically aligned SWNT "carpets" produced using the method described by Xu et al.[53] The carpets typically consisted of 20−200 μm long vertical array of SWNTs bound to Fe catalyst particles and supported on Silicon substrates, as shown in Figure 1a. Thin films were obtained from the SWNT carpets using a modified version of the "roll-over" method.[54] In short, vertically aligned SWNTs were "tilted" toward the desired direction of alignment by gentle unidirectional rubbing with a clean strip of velvet cloth, followed by the "rolling" process which compresses the carpet into a dense, highly aligned SWNT film (Figure 1b). A thin sheet of aluminum foil was used during rolling to prevent transfer of any SWNTs from the carpet on to the roller. Dipping these SWNT films in 1 M HCl solution etches away the catalyst particles, resulting in their immediate detachment from Silicon substrates; the free floating films can then be transferred onto any desired substrate.

SWNT fibers were produced by wet spinning from high concentration (>8 wt %) SWNT-Oleum (100% sulfuric acid + 20% SO_3) solutions.[25,55−58] Polarized Raman spectroscopy of the fiber showed that for the so-called G peak (∼1591 cm^{-1}) the ratio of intensities measured for polarizations in longitudinal vs transverse directions is about 2.4, indicating a high degree of SWNT alignment, further confirmed by SEM (Figure 2a). SEM was performed using a (JEOL JSM-7401F FESEM).

■ ASSOCIATED CONTENT

ⓢ Supporting Information. Order parameter calculation, typical error in measurements, and SEM images of single and multiple rounds of GNR deposition on SWNT film and fibers. This material is available free of charge via the Internet at http://pubs.acs.org/.

■ AUTHOR INFORMATION

Corresponding Author
*E-mail: mp@rice.edu (M.P.); ivan.smalyukh@colorado.edu (I.I.S.).

■ ACKNOWLEDGMENT

■ REFERENCES

(1) Daniel, M. C.; Astruc, D. *Chem. Rev.* **2004**, *104* (1), 293–346.

(2) Murphy, C. J.; San, T. K.; Gole, A. M.; Orendorff, C. J.; Gao, J. X.; Gou, L.; Hunyadi, S. E.; Li, T. *J. Phys. Chem. B* **2005**, *109* (29), 13857–13870.

(3) Link, S.; Mohamed, M. B.; El-Sayed, M. A. *J. Phys. Chem. B* **1999**, *103* (16), 3073–3077.

(4) Westphalen, M.; Kreibig, U.; Rostalski, J.; Luth, H.; Meissner, D. *Sol. Energy Mater. Sol. Cells* **2000**, *61* (1), 97–105.

(5) Atwater, H. A.; Polman, A. *Nat. Mater.* **2010**, *9* (3), 205–213.

(6) Morfa, A. J.; Rowlen, K. L.; Reilly, T. H.; Romero, M. J.; van de Lagemaat, J. *Appl. Phys. Lett.* **2008**, *92* (1), 013504.

(7) Orendorff, C. J.; Gearheart, L.; Jana, N. R.; Murphy, C. J. *Phys. Chem. Chem. Phys.* **2006**, *8* (1), 165–170.

(8) Nikoobakht, B.; El-Sayed, M. A. *J. Phys. Chem. A* **2003**, *107* (18), 3372–3378.

(9) Huang, X. H.; El-Sayed, I. H.; Qian, W.; El-Sayed, M. A. *J. Am. Chem. Soc.* **2006**, *128* (6), 2115–2120.

(10) Huang, X. H.; El-Sayed, I. H.; Qian, W.; El-Sayed, M. A. *Nano Lett.* **2007**, 7 (6), 1591–1597.

(11) Durr, N. J.; Larson, T.; Smith, D. K.; Korgel, B. A.; Sokolov, K.; Ben-Yakar, A. *Nano Lett.* **2007**, 7 (4), 941–945.

(12) Liu, Q. K.; Cui, Y. X.; Gardner, D.; Li, X.; He, S. L.; Smalyukh, I. *Nano Lett.* **2010**, *10* (4), 1347–1353.

(13) Shalaev, V. M.; Cai, W. S.; Chettiar, U. K.; Yuan, H. K.; Sarychev, A. K.; Drachev, V. P.; Kildishev, A. V. *Opt. Lett.* **2005**, *30* (24), 3356–3358.

(14) Shenhar, R.; Norsten, T. B.; Rotello, V. M. *Adv. Mater.* **2005**, *17* (6), 657–669.

(15) Murphy, C. L.; Orendorff, C. J. *Adv. Mater.* **2005**, *17* (18), 2173–2177.

(16) van der Zande, B. M. I.; Koper, G. J. M.; Lekkerkerker, H. N. W. *J. Phys. Chem. B* **1999**, *103* (28), 5754–5760.

(17) Jana, N. R.; Gearheart, L. A.; Obare, S. O.; Johnson, C. J.; Edler, K. J.; Mann, S.; Murphy, C. J. *J. Mater. Chem.* **2002**, *12* (10), 2909–2912.

(18) Nikoobakht, B.; Wang, Z. L.; El-Sayed, M. A. *J. Phys. Chem. B* **2000**, *104* (36), 8635–8640.

(19) Liu, S. H.; Tok, J. B. H.; Locklin, J.; Bao, Z. N. *Small* **2006**, *2* (12), 1448–1453.

(20) Green, M. J.; Behabtu, N.; Pasquali, M.; Adams, W. W. *Polymer* **2009**, *50* (21), 4979–4997.

(21) Tans, S. J.; Devoret, M. H.; Dai, H. J.; Thess, A.; Smalley, R. E.; Geerligs, L. J.; Dekker, C. *Nature* **1997**, *386* (6624), 474–477.

(22) Dan, B.; Irvin, G. C.; Pasquali, M. *ACS Nano* **2009**, *3* (4), 835–843.

(23) Wu, Z. C.; Chen, Z. H.; Du, X.; Logan, J. M.; Sippel, J.; Nikolou, M.; Kamaras, K.; Reynolds, J. R.; Tanner, D. B.; Hebard, A. F.; Rinzler, A. G. *Science* **2004**, *305* (5688), 1273–1276.

(24) Behabtu, N.; Green, M. J.; Pasquali, M. *Nano Today* **2008**, *3* (5–6), 24–34.

(25) Davis, V. A.; Parra-Vasquez, A. N. G.; Green, M. J.; Rai, P. K.; Behabtu, N.; Prieto, V.; Booker, R. D.; Schmidt, J.; Kesselman, E.; Zhou, W.; Fan, H.; Adams, W. W.; Hauge, R. H.; Fischer, J. E.; Cohen, Y.; Talmon, Y.; Smalley, R. E.; Pasquali, M. *Nat. Nanotechnol.* **2009**, *4* (12), 830–834.

(26) Li, Y. L.; Kinloch, I. A.; Windle, A. H. *Science* **2004**, *304* (5668), 276–278.

(27) Miaudet, P.; Badaire, S.; Maugey, M.; Derre, A.; Pichot, V.; Launois, P.; Poulin, P.; Zakri, C. *Nano Lett.* **2005**, *5* (11), 2212–2215.

(28) Hu, L.; Hecht, D. S.; Gruner, G. *Chem. Rev.* **2010**, *110* (10), 5790–844.

(29) Kong, B. S.; Jung, D. H.; Oh, S. K.; Han, C. S.; Jung, H. T. *J. Phys. Chem. C* **2007**, *111* (23), 8377–8382.

(30) Peigney, A.; Laurent, C.; Flahaut, E.; Bacsa, R. R.; Rousset, A. *Carbon* **2001**, *39* (4), 507–514.

(31) Girishkumar, G.; Vinodgopal, K.; Kamat, P. V. *J.Phys. Chem. B* **2004**, *108* (52), 19960–19966.

(32) Planeix, J. M.; Coustel, N.; Coq, B.; Brotons, V.; Kumbhar, P. S.; Dutartre, R.; Geneste, P.; Bernier, P.; Ajayan, P. M. *J. Am. Chem. Soc.* **1994**, *116* (17), 7935–7936.

(33) Correa-Duarte, M. A.; Perez-Juste, J.; Sanchez-Iglesias, A.; Giersig, M.; Liz-Marzan, L. M. *Angew. Chem.,Int. Ed.* **2005**, *44* (28), 4375–4378.

(34) Yang, D.-K.; Wu, S.-T., *Fundamentals of Liquid Crystal Devices*; John Wiley: Hoboken, NJ, 2006.

(35) Collings, P. J.; Ratna, B. R.; Shashidhar, R. *Phys. Rev. E* **2003**, *67* (2), 21705.

(36) Smalyukh, I. I.; Butler, J.; Shrout, J. D.; Parsek, M. R.; Wong, G. C. L. *Phys. Rev. E* **2008**, *78* (3), 30701.

(37) Lapointe, C. P.; Mason, T. G.; Smalyukh, I. I. *Science* **2009**, *326* (5956), 1083–1086.

(38) Evans, J. S.; Beier, C.; Smalyukh, I. I. *J. Appl. Phys.* **2011**, *110*, 033535.

(39) Deegan, R. D.; Bakajin, O.; Dupont, T. F.; Huber, G.; Nagel, S. R.; Witten, T. A. *Nature* **1997**, *389* (6653), 827–829.

(40) Li, Q. W.; Zhu, Y. T.; Kinloch, I. A.; Windle, A. H. *J. Phys. Chem. B* **2006**, *110* (28), 13926–13930.

(41) Lewandowski, E. P.; Bernate, J. A.; Searson, P. C.; Stebe, K. J. *Langmuir* **2008**, *24* (17), 9302–9307.

(42) Fan, F. Q.; Stebe, K. J. *Langmuir* **2004**, *20* (8), 3062–3067.

(43) Sharma, R.; Lee, C. Y.; Choi, J. H.; Chen, K.; Strano, M. S. *Nano Lett.* **2007**, *7* (9), 2693–2700.

(44) Petit, C. A. P.; Carbeck, J. D. *Nano Lett.* **2003**, *3* (8), 1141–1146.

(45) Messer, B.; Song, J. H.; Yang, P. D. *J. Am. Chem. Soc.* **2000**, *122* (41), 10232–10233.

(46) Salalha, W.; Zussman, E. *Phys. Fluids* **2005**, *17* (6), 063301.

(47) Berreman, D. W. *Phys. Rev. Lett.* **1972**, *28* (26), 1683–1686.

(48) Dinsmore, A. D.; Yodh, A. G.; Pine, D. J. *Nature* **1996**, *383* (6597), 239–242.

(49) Gupta, S.; Zhang, Q. L.; Emrick, T.; Balazs, A. C.; Russell, T. P. *Nat. Mater.* **2006**, *5* (3), 229–233.

(50) Yodh, A. G.; Lin, K. H.; Crocker, J. C.; Dinsmore, A. D.; Verma, R.; Kaplan, P. D. *Philos. T.rans. R. Soc. Chem., Ser. A* **2001**, *359* (1782), 921–937.

(51) Onsager, L. *Ann. N.Y. Acad. Sci.* **1949**, *51* (4), 627–659.

(52) Chandran, S. P.; Chaudhary, M.; Pasricha, R.; Ahmad, A.; Sastry, M. *Biotechnol. Prog.* **2006**, *22* (2), 577–583.

(53) Xu, Y. Q.; Flor, E.; Kim, M. J.; Hamadani, B.; Schmidt, H.; Smalley, R. E.; Hauge, R. H. *J. Am. Chem. Soc.* **2006**, *128* (20), 6560–6561.

(54) Pint, C. L.; Xu, Y. Q.; Pasquali, M.; Hauge, R. H. *ACS Nano* **2008**, *2* (9), 1871–1878.

(55) Ericson, L. M.; Fan, H.; Peng, H. Q.; Davis, V. A.; Zhou, W.; Sulpizio, J.; Wang, Y. H.; Booker, R.; Vavro, J.; Guthy, C.; Parra-Vasquez, A. N. G.; Kim, M. J.; Ramesh, S.; Saini, R. K.; Kittrell, C.; Lavin, G.; Schmidt, H.; Adams, W. W.; Billups, W. E.; Pasquali, M.; Hwang, W. F.; Hauge, R. H.; Fischer, J. E.; Smalley, R. E. *Science* **2004**, *305* (5689), 1447–1450.

(56) Wang, Y.; Ericson, L. M.; Kittrell, C.; Kim, M. J.; Shan, H.; Fan, H.; Ripley, S.; Ramesh, S.; Hauge, R. H.; Adams, W. W.; Pasquali, M.; Smalley, R. E. *Chem. Mater.* **2005**, *17* (25), 6361–6368.

(57) Booker, R.; Green, M.; Fan, H.; Parra-Vasquez, A.; Behabtu, N.; Young, C.; Hauge, R.; Schmidt, H.; Smalley, R.; Hwang, W.; Pasquali, M. *Proc. Inst.Mech. Eng., Part N: J. Nanoeng. Nanosyst.* **2008**, *222* (3), 101–109.

(58) Davis, V. A.; Ericson, L. M.; Parra-Vasquez, A. N. G.; Fan, H.; Wang, Y. H.; Prieto, V.; Longoria, J. A.; Ramesh, S.; Saini, R. K.; Kittrell, C.; Billups, W. E.; Adams, W. W.; Hauge, R. H.; Smalley, R. E.; Pasquali, M. *Macromolecules* **2004**, *37* (1), 154–160.